Research Article | Vol. 7, No. 10 | 1 Oct 2017 | OPTICAL MATERIALS EXPRESS 3643
Optical Materials EXPRESS

High-sensitivity β-Ga_2O_3 solar-blind photodetector on high-temperature pretreated c-plane sapphire substrate

Ling-Xuan Qian,[1,4] Hua-Fan Zhang,[2] P. T. Lai,[3] Ze-Han Wu,[1] and Xing-Zhao Liu[1,5]

[1]*State Key Laboratory of Electronic Thin Films and Integrated Devices, School of Microelectronics and Solid-State Electronics, University of Electronic Science and Technology of China, Chengdu 611731, China*
[2]*Photonics Laboratory, King Abdullah University of Science and Technology, Thuwal 23955-6900, Saudi Arabia*
[3]*Department of Electrical and Electronic Engineering, The University of Hong Kong, Pokfulam Road, Hong Kong, Hong Kong*
[4]*lxqian@uestc.edu.cn*
[5]*xzliu@uestc.edu.cn*

Abstract: Recently, monoclinic Ga_2O_3 (β-Ga_2O_3) photodetectors (PDs) have been extensively studied for various commercial and military applications due to the merits of intrinsic solar rejection, high gain, and great compactness. In this work, c-plane sapphire substrates were annealed under different temperatures in a vacuum furnace prior to the molecular beam epitaxy (MBE) of β-Ga_2O_3 thin film, which yielded a smoother surface and even a terrace-and-step-like morphology on the substrate, resulting in improved crystallinity of the epitaxial film. Accordingly, both the dark and photo currents of β-Ga_2O_3 metal-semiconductor-metal (MSM) PDs were increased by the enhanced carrier mobility (μ) of the more crystalline film. However, the substrate-annealing temperature must be sufficiently high to offset the rise of the dark current and thus achieve a remarkable improvement in the photodetection properties. As a result, the PD fabricated on the 1050 °C-annealed substrate exhibited extremely high sensitivity, for example, high responsivity (R) of 54.9 A/W and large specific detectivity (D*) of 3.71×10^{14} Jones. Both parameters were increased by one order of magnitude because of the combined effects of the dramatic increase in μ and the effective reduction in defect-related recombination centers. Nevertheless, the latter also prolonged the recovery time of the PD. These findings suggest another way to develop β-Ga_2O_3 PD with extremely high sensitivity.

OCIS codes: (040.5160) Photodetectors; (040.7190) Ultraviolet; (160.6000) Semiconductor materials; (310.6845) Thin film devices and applications

References and links

1. Z. Alaie, S. Mohammad Nejad, and M. H. Yousefi, "Recent advances in ultraviolet photodetectors," Mater. Sci. Semicond. Process. **29**, 16–55 (2015).
2. E. Monroy, F. Omnès, and F. Calle, "Wide-bandgap semiconductor ultraviolet photodetectors," Semicond. Sci. Technol. **18**(4), R33–R51 (2003).
3. W. Zhang, J. Xu, W. Ye, Y. Li, Z. Qi, J. Dai, Z. Wu, C. Chen, J. Yin, J. Li, H. Jiang, and Y. Fang, "High-performance AlGaN metal–semiconductor–metal solar-blind ultraviolet photodetectors by localized surface plasmon enhancement," Appl. Phys. Lett. **106**(2), 021112 (2015).
4. Y. Hou, Z. Mei, and X. Du, "Semiconductor ultraviolet photodetectors based on ZnO and $Mg_xZn_{1-x}O$," J. Phys. D Appl. Phys. **47**(28), 283001 (2014).
5. Y. Koide, M. Liao, and J. Alvarez, "Thermally stable solar-blind diamond UV photodetector," Diamond Related Materials **15**(11-12), 1962–1966 (2006).
6. R.-Y. Yang, C.-M. Hsiung, H.-H. Chen, H.-W. Wu, and M.-C. Shih, "Effect of AIN film thickness on photo/dark currents of MSM UV photodetector," Microw. Opt. Technol. Lett. **50**(11), 2863–2866 (2008).
7. L. Sang, M. Liao, and M. Sumiya, "A comprehensive review of semiconductor ultraviolet photodetectors: from thin film to one-dimensional nanostructures," Sensors (Basel) **13**(8), 10482–10518 (2013).

#303061 https://doi.org/10.1364/OME.7.003643
Journal © 2017 Received 21 Jul 2017; revised 11 Sep 2017; accepted 16 Sep 2017; published 20 Sep 2017

Optical Materials EXPRESS

8. X. Du, Z. Mei, Z. Liu, Y. Guo, T. Zhang, Y. Hou, Z. Zhang, Q. Xue, and A. Y. Kuznetsov, "Controlled Growth of High-Quality ZnO-Based Films and Fabrication of Visible-Blind and Solar-Blind Ultra-Violet Detectors," Adv. Mater. **21**(45), 4625–4630 (2009).
9. Y. H. An, D. Y. Guo, S. Y. Li, Z. P. Wu, Y. Q. Huang, P. G. Li, L. H. Li, and W. H. Tang, "Influence of oxygen vacancies on the photoresponse of β-Ga_2O_3/SiC n–n type heterojunctions," J. Phys. D Appl. Phys. **49**(28), 285111 (2016).
10. R. Suzuki, S. Nakagomi, and Y. Kokubun, "Solar-blind photodiodes composed of a Au Schottky contact and a β-Ga_2O_3 single crystal with a high resistivity cap layer," Appl. Phys. Lett. **98**(13), 131114 (2011).
11. D. Guo, H. Liu, P. Li, Z. Wu, S. Wang, C. Cui, C. Li, and W. Tang, "Zero-Power-Consumption Solar-Blind Photodetector Based on β-Ga_2O_3/NSTO Heterojunction," ACS Appl. Mater. Interfaces **9**(2), 1619–1628 (2017).
12. S. Oh, J. Kim, F. Ren, S. J. Pearton, and J. Kim, "Quasi-two-dimensional β-gallium oxide solar-blind photodetectors with ultrahigh responsivity," J. Mater. Chem. C Mater. Opt. Electron. Devices **4**(39), 9245–9250 (2016).
13. S. Oh, Y. Jung, M. A. Mastro, J. K. Hite, C. R. Eddy, Jr., and J. Kim, "Development of solar-blind photodetectors based on Si-implanted β-Ga_2O_3," Opt. Express **23**(2), 28300–28305 (2015).
14. S. Nakagomi and Y. Kokubun, "Crystal orientation of β-Ga_2O_3 thin films formed on c-plane and a-plane sapphire substrate," J. Cryst. Growth **349**(1), 12–18 (2012).
15. D. Guo, Z. Wu, P. Li, Y. An, H. Liu, X. Guo, H. Yan, G. Wang, C. Sun, L. Li, and W. Tang, "Fabrication of β-Ga_2O_3 thin films and solar-blind photodetectors by laser MBE technology," Opt. Mater. Express **4**(5), 1067 (2014).
16. G. Shukla and A. Khare, "Effect of substrate annealing on the quality of pulsed laser deposited $Zn_{1-x}Mg_xO$ thin films," Appl. Surf. Sci. **255**(15), 7017–7020 (2009).
17. M. A. Boukadhaba, A. Fouzri, V. Sallet, S. S. Hassani, G. Amiri, A. Lusson, and M. Oumezzine, "High-temperature annealing effect of α-Al_2O_3 (0001) substrates with nominal 0.25° miscut toward the a-plane (–1120) on ZnO films grown by MOCVD," Appl. Phys., A Mater. Sci. Process. **120**(3), 991–1000 (2015).
18. W.-C. Lien, D.-S. Tsai, D.-H. Lien, D. G. Senesky, J.-H. He, and A. P. Pisano, "4H-SiC Metal-Semiconductor-Metal Ultraviolet Photodetectors in Operation of 450·C," IEEE Electron Device Lett. **33**(11), 1586–1588 (2012).
19. F. Cuccureddu, S. Murphy, I. V. Shvets, M. Porcu, H. W. Zandbergen, N. S. Sidorov, and S. I. Bozhko, "Surface morphology of c-plane sapphire (α-alumina) produced by high temperature anneal," Surf. Sci. **604**(15), 1294–1299 (2010).
20. M. Yoshimoto, T. Maeda, T. Ohnishi, H. Koinuma, O. Ishiyama, M. Shinohara, M. Kubo, R. Miura, and A. Miyamoto, "Atomic-scale formation of ultrasmooth surfaces on sapphire substrates for high-quality thin-film fabrication," Appl. Phys. Lett. **67**(18), 2615–2617 (1995).
21. H. G. Jiang, M. Ruhle, and E. J. Lavernia, "On the applicability of the x-ray diffraction line profile analysis in extracting grain size and microstrain in nanocrystalline materials," J. Mater. Res. **14**(02), 549–559 (1999).
22. C. V. Ramana, E. J. Rubio, C. D. Barraza, A. Miranda Gallardo, S. McPeak, S. Kotru, and J. T. Grant, "Chemical bonding, optical constants, and electrical resistivity of sputter-deposited gallium oxide thin films," J. Appl. Phys. **115**(4), 043508 (2014).
23. R. S. Vemuri, K. K. Bharathi, S. K. Gullapalli, and C. V. Ramana, "Effect of structure and size on the electrical properties of nanocrystalline WO_3 films," ACS Appl. Mater. Interfaces **2**(9), 2623–2628 (2010).
24. J. C. Carrano, T. Li, P. A. Grudowski, C. J. Eiting, R. D. Dupuis, and J. C. Campbell, "Comprehensive characterization of metal–semiconductor–metal ultraviolet photodetectors fabricated on single-crystal GaN," J. Appl. Phys. **83**(11), 6148–6160 (1998).
25. H. Huang, W. Yang, Y. Xie, X. Chen, and Z. Wu, "Metal-Semiconductor-Metal Ultraviolet Photodetectors Based on TiO_2 Films Deposited by Radio-Frequency Magnetron Sputtering," IEEE Electron Device Lett. **31**(6), 588–590 (2010).
26. Q. N. Abdullah, F. K. Yam, K. H. Mohmood, Z. Hassan, M. A. Qaeed, M. Bououdina, M. A. Almessiere, A. L. Al-Otaibi, and S. A. Abdulateef, "Free growth of one-dimensional β-Ga_2O_3 nanostructures including nanowires, nanobelts and nanosheets using a thermal evaporation method," Ceram. Int. **42**(12), 13343–13349 (2016).
27. M. D. Heinemann, J. Berry, G. Teeter, T. Unold, and D. Ginley, "Oxygen deficiency and Sn doping of amorphous Ga_2O_3," Appl. Phys. Lett. **108**(2), 022107 (2016).
28. V. N. Sigaev, N. V. Golubev, E. S. Ignat'eva, A. Paleari, and R. Lorenzi, "Light-emitting Ga-oxide nanocrystals in glass: a new paradigm for low-cost and robust UV-to-visible solar-blind converters and UV emitters," Nanoscale **6**(3), 1763–1774 (2014).
29. X. Gong, M. Tong, Y. Xia, W. Cai, J. S. Moon, Y. Cao, G. Yu, C. L. Shieh, B. Nilsson, and A. J. Heeger, "High-Detectivity Polymer Photodetectors with Spectral Response from 300 nm to 1450 nm," Science **325**(5948), 1665–1667 (2009).
30. W. Y. Kong, G. A. Wu, K. Y. Wang, T. F. Zhang, Y. F. Zou, D. D. Wang, and L. B. Luo, "Graphene-β-Ga_2O_3 Heterojunction for Highly Sensitive Deep UV Photodetector Application," Adv. Mater. **28**(48), 10725–10731 (2016).
31. F.-P. Yu, S.-L. Ou, and D.-S. Wuu, "Pulsed laser deposition of gallium oxide films for high performance solar-blind photodetectors," Opt. Mater. Express **5**(5), 1240–1249 (2015).
32. G. C. Hu, C. X. Shan, N. Zhang, M. M. Jiang, S. P. Wang, and D. Z. Shen, "High gain Ga_2O_3 solar-blind photodetectors realized via a carrier multiplication process," Opt. Express **23**(10), 13554–13561 (2015).

Optical Materials EXPRESS

33. R. Yukawa, S. Yamamoto, K. Ozawa, M. Emori, M. Ogawa, S. Yamamoto, K. Fujikawa, R. Hobara, S. Kitagawa, H. Daimon, H. Sakama, and I. Matsuda, "Electron-hole recombination on ZnO(0001) single-crystal surface studied by time-resolved soft X-ray photoelectron spectroscopy," Appl. Phys. Lett. **105**(15), 151602 (2014).

1. Introduction

Photodetectors that only sense radiation with wavelengths shorter than 280 nm are usually classified as solar-blind PDs because photons in this deep-ultraviolet (DUV) region of solar radiation seldom reach the Earth's surface due to strong absorption by the stratospheric ozone layer. Accordingly, solar-blind PDs can respond accurately to a very weak signal, even under sun or room illumination, and thus have an incomparable advantage over conventional UV PDs, especially for certain special applications, such as ozone-hole monitoring, fire detection, and missile threat warning [1, 2]. Recently, solid-state PDs based on wide-bandgap semiconductors, including AlGaN [3], ZnMgO [4], diamond [5], and AlN [6], have been extensively explored for applications of solar-blind photodetection owing to their small size, light weight and low power consumption. However, the proportion of Al in AlGaN must exceed 40% to achieve a sufficiently large bandgap, which can generate high-density structural defects due to the slower atomic migration of Al than Ga and strong parasitic reactions [7]. Similarly, the phase segregations of ZnO wurtzite and MgO rock salt in Mg-rich ZnMgO make it difficult to achieve a bandgap larger than 4.5 eV [8]. The sensitivity ranges of diamond and AlN are confined to narrow radiation regions due to a fixed bandgap of ~5.5 eV and ~6.2 eV, respectively [5, 7, 9]. In comparison, monoclinic Ga_2O_3 (β-Ga_2O_3) possesses an intrinsic E_g of 4.9 eV, corresponding to a wavelength of ~260 nm. Therefore, this PD is suitable for solar-blind detection without the need of any alloying process, making β-Ga_2O_3 PDs better alternatives that have attracted considerable attention in the past decade [10–13]. In general, the photodetection characteristics of thin-film-type PD rely on the crystalline quality of epitaxial film, which is readily influenced by different factors. Accordingly, researchers have attempted improve the crystalline quality of β-Ga_2O_3 thin films. For example, the c-plane (0001) of sapphire substrates are often adopted for the epitaxial growth of β-Ga_2O_3 thin films due to the high similarity in the oxygen-atom arrangement between the β-Ga_2O_3 ($\bar{2}$01) plane and the sapphire c-plane [14]. Moreover, process conditions, for example, substrate temperature, oxygen pressure, and post-deposition annealing, have to be carefully optimized [15].

In fact, there are often many defects on the topmost surface of as-supplied sapphire substrates, for example, scratches, irregular corrugation and crystallographic defects, which are caused by mechano-chemical mirror polishing. In addition, a mis-orientation inclined from the atomic plane with a small angle ($<0.5°$) occurs unavoidably due to the limited precision of cutting machinery. As a consequence, the crystal quality of the β-Ga_2O_3 epitaxial film could be degraded because the coherence degree at the interface between the epitaxial film and substrate greatly impacts defect formation, strain transfer and evolution of the film surface. Pretreatment of sapphire substrate by thermal annealing has been reported to effectively improve the crystal quality of ZnO and ZnMgO epitaxial films [16, 17]. However, few studies have systematically investigated the effects of similar pretreatment on the crystal quality of β-Ga_2O_3 epitaxial film or the performance of β-Ga_2O_3 PD.

In this work, β-Ga_2O_3 thin films were epitaxially grown on c-plane sapphire substrates by plasma-assisted MBE. Beforehand, thermal annealing of c-plane sapphire substrates was performed at different temperatures in a tubular furnace under vacuum to repair their defective surfaces. Based on the epitaxial films, MSM PDs were fabricated because of their high responsivity, large photocurrent gain, easy integration with readout circuitry, and other characteristics [18]. Moreover, another MSM PD based on a β-Ga_2O_3 thin film deposited on the as-supplied c-plane sapphire was also prepared as the control sample. Accordingly, both the structural properties of β-Ga_2O_3 epitaxial films and the characteristics of related MSM

Optical Materials EXPRESS

PDs were comprehensively investigated, and extremely high sensitivity was achieved by the PD fabricated on the 1050 °C-annealed substrate.

2. Experimental details

First, sapphire substrates were annealed in a tubular furnace for 120 min, during which time the vacuum level was maintained at 3.0×10^{-4} Pa and the ambient temperatures were fixed at 600 °C, 750 °C, 900 °C and 1050 °C, depending on the sample. Second, β-Ga_2O_3 thin films with a thickness of ~100 nm were simultaneously deposited on the as-supplied and annealed substrates by plasma-assisted MBE using optimized process conditions: a base pressure of 3.0×10^{-8} Torr, Ga Knudsen cell temperature of 940 °C, substrate-heating temperature of 760 °C, input radio-frequency (RF) power of 300 W, and O_2 flow rate of 2 sccm. Next, MSM PDs were fabricated using the conventional lift-off process. Each device had 20 pairs of interdigital electrodes with length, width and spacing of 180 μm, 5 μm and 5 μm, respectively; as a result, the effective illumination area was 3.8×10^{-4} cm^2. In addition, each electrode consisted of 20-nm Ti and 80-nm Al, both grown by electron beam evaporation. The thin Ti layer was employed to improve both the adhesion and the electrical contact of Al on the β-Ga_2O_3 thin film. Finally, all samples were annealed at 500 °C for 5 min in a N_2 ambient to further reduce the contact resistance of the electrodes. The epitaxially grown Ga_2O_3 films herein are referred to as Film-0, Film-600, Film-750, Film-900 and Film-1050, while the fabricated devices are named PD-0, PD-600, PD-750, PD-900 and PD-1050 based on the different substrate-annealing temperatures.

The surface morphologies of the sapphire substrates and subsequently deposited β-Ga_2O_3 epitaxial films were determined by a Seiko Instruments SPA-300 HV atomic force microscope (AFM). Moreover, the crystallinity of the β-Ga_2O_3 epitaxial films was monitored by a Bede D1 X-ray diffractometer (XRD). For the device characteristics, the current-voltage (I-V) and transient response were measured using an Agilent 4155B semiconductor parameter analyzer, with a low-pressure mercury lamp combined with a 254-nm filter as the UV light source. The spectral response was measured using a Zolix DSR100-X150AUV automated spectro-radiometric measurement system.

3. Results and discussion

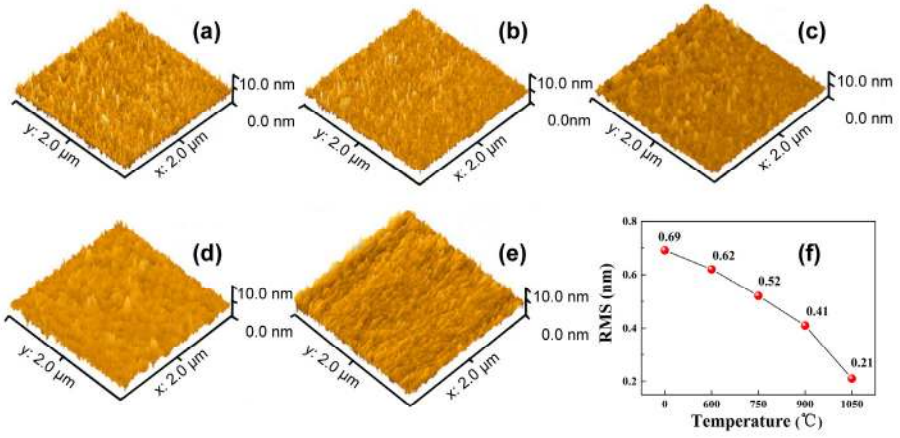

Fig. 1. 3D AFM images of c-plane sapphire substrates annealed at (a) NA, (b) 600 °C, (c) 750 °C, (d) 900 °C and (e) 1050 °C. (f) Plot of RMS versus annealing temperature.

Figure 1 demonstrates the three-dimensional (3D) AFM images of the c-plane sapphire substrates annealed at various temperatures. Smoother substrate surfaces are achieved by thermal-annealing pretreatment compared to the as-supplied substrate. Accordingly, the root-

Optical Materials EXPRESS

mean-square (RMS) values are 0.69 nm, 0.62 nm, 0.52 nm, 0.41 nm, and 0.21 nm for the as-supplied, 600 °C-annealed, 750 °C-annealed, 900 °C-annealed, and 1050 °C-annealed substrates, respectively. As shown in Fig. 1(f), the RMS value exhibits a monotonically decreasing trend with increasing annealing temperatures. Moreover, despite poorly defined terrace edges, a similar terrace-and-step morphology appears on the 1050 °C-annealed substrate, which is similar to previously reported results [17, 19]. It was reported that there are several ordered phases on the c-plane surface of sapphire that can transform into each other under thermal treatment [19]. Hence, these observations are attributed to the reconstruction of the crystal structure on the surface of the sapphire substrate due to the high-temperature-enhanced atom migration and minimization of surface energy [20].

Figure 2(a) demonstrates the out-of-plane XRD spectra of Ga_2O_3 epitaxial films grown on the sapphire substrates with different annealing temperatures. For each sample, all peaks correspond to β-Ga_2O_3 ($\bar{2}$ 01) and the corresponding higher-order diffractions (located at 18.88°, 38.26°, and 58.96°), except those from the sapphire substrate (JCPDS CARD No. 43–1012), indicate a single-phase structure with ($\bar{2}$ 01) preferred orientation. Moreover, all the diffraction intensities are normalized based on the diffraction peak corresponding to the sapphire (0006) plane. More intense ($\bar{2}$ 01) diffraction peaks at 2θ = 18.88° are observed for β-Ga_2O_3 epitaxial films grown on the annealed substrates than those grown on the as-supplied substrate. This effect is enhanced by the rise of the annealing temperature. Furthermore, the values for the full width at half maximum (FWHM) of the ($\bar{2}$ 01) diffraction peaks are 0.305°, 0.268°, 0.261°, 0.260°, and 0.240° for Film-0, Film-600, Film-750, Film-900, and Film-1050, respectively. Accordingly, the crystallite sizes (D) are deduced based on the Scherrer equation [21]:

$$D = 0.9\lambda' / \beta \cos\theta \quad (1)$$

where λ' is the X-ray wavelength (Cu Kα source, 1.5418 Å), β the FWHM in radians, and θ the Bragg angle. The estimated D values are 26.43 nm, 30.07 nm, 30.88 nm, 31.00 nm, and 33.58 nm for Film-0, Film-600, Film-750, Film-900, and Film-1050, respectively. Clearly, the crystallinity of the β-Ga_2O_3 epitaxial film is effectively improved by annealing the substrate, and this effect becomes more evident at higher annealing temperatures. Figure 2(b) demonstrates the X-ray rocking curves of the ($\bar{2}$ 01) diffraction peaks for the samples, and the corresponding FWHM values are 2.2°, 2.0°, 1.5°, 1.2°, and 0.8° for Film-0, Film-600, Film-750, Film-900, and Film-1050, respectively. This figure further confirms the improved crystallinity of β-Ga_2O_3 epitaxial films grown on the annealed sapphire substrates; Film-1050 has the highest degree of crystallinity. These observations are consistent with a previous report in which the high-temperature phase of sapphire surface with a terrace-and-step morphology was demonstrated to facilitate nucleation during film growth [16].

Optical Materials EXPRESS

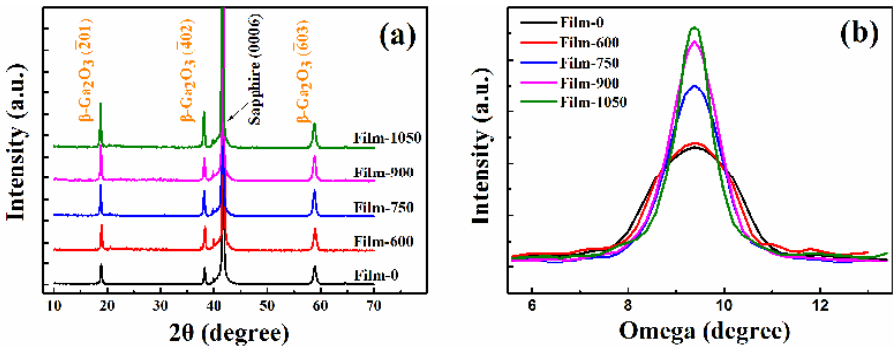

Fig. 2. XRD spectra of β-Ga_2O_3 epitaxial films grown on c-plane sapphire substrates with different thermal-annealing pretreatments: (a) θ-2θ and (b) Omega scans.

Figure 3 demonstrates the AFM results for β-Ga_2O_3 epitaxy films grown on the sapphire substrates with different annealing temperatures. As shown in Fig. 3(a), there is an obvious nanoparticulate morphology on the surface of Film-0, where the conically shaped grains are distributed uniformly. For the annealed substrates, the grain size increases, and the island-like structure tends to appear, which is more conspicuous for higher substrate-annealing temperatures. This observation is in good agreement with the XRD results and further confirms the improved crystallinity of β-Ga_2O_3 epitaxy film by adopting the annealed substrate. This effect is also reflected by the change in surface roughness [22], and the RMS value monotonically increases from 1.35 to 3.17 nm with increasing substrate-annealing temperatures, as shown in Fig. 3(f). It might be attributed to the increased grain size.

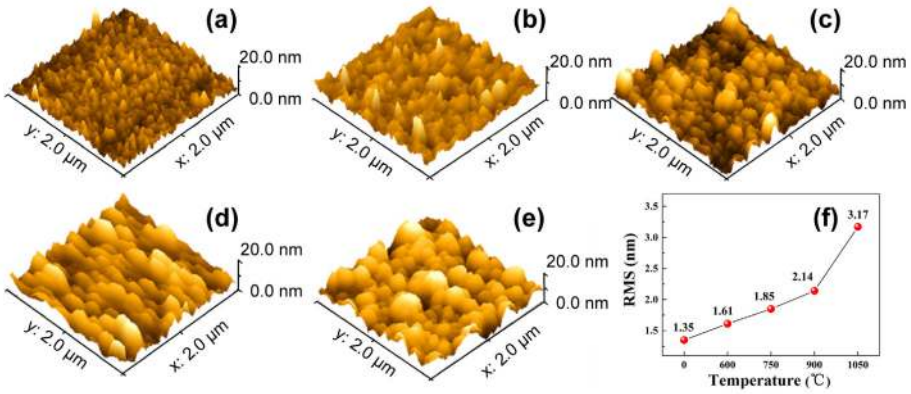

Fig. 3. AFM 3D images of β-Ga_2O_3 epitaxial films grown on (a) as-supplied, (b) 600 °C-annealed, (c) 750 °C-annealed, (d) 900 °C-annealed and (e) 1050 °C-annealed c-plane sapphire substrates. (f) Plot of RMS versus annealing temperature.

Optical Materials EXPRESS

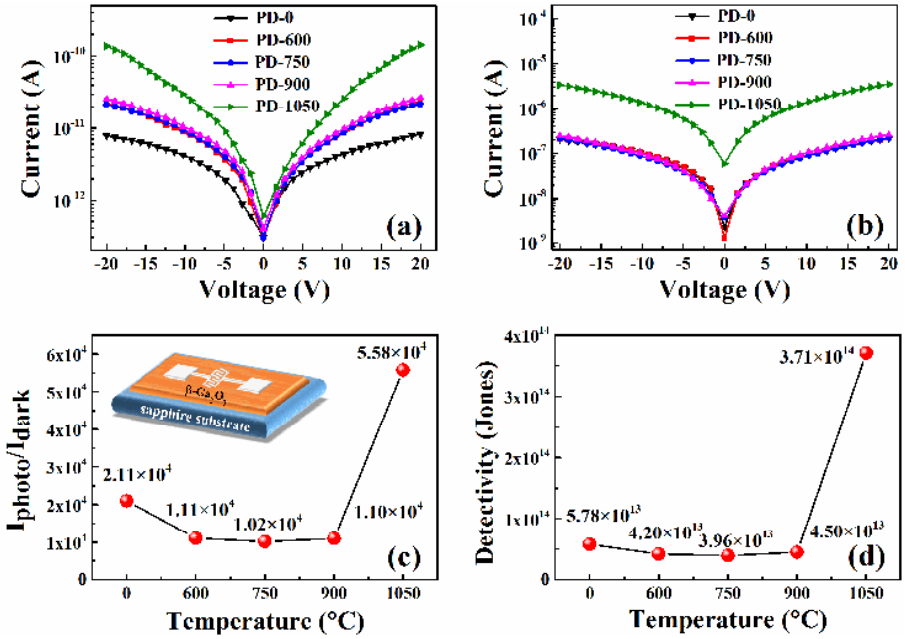

Fig. 4. I-V characteristics of β-Ga_2O_3 MSM PDs based on the as-supplied and annealed c-plane sapphire substrates (a) in dark, and (b) under DUV radiation; (c) current ratio and (d) detectivity. Inset of (c) is the schematic diagram of β-Ga_2O_3 MSM PD.

Figure 4 presents the semi-logarithmic I-V plots of the β-Ga_2O_3 PDs based on sapphire substrates with different annealing temperatures, which are characterized in the dark and under 69.5-μW/cm^2 and 254-nm UV illumination. As shown in Fig. 4(a), the dark current (I_{dark}) becomes much larger if adopting the annealed substrates, and this effect is more prominent for the highest substrate-annealing temperature of 1050 °C. Oxygen vacancies act as donor states in β-Ga_2O_3, and their density can impact the intrinsic carrier concentration and thus electrical conductivity. Considering that the β-Ga_2O_3 thin films were grown simultaneously under the same conditions for all the samples, we attribute the relatively large I_{dark} to the increased carrier mobility (μ) of the β-Ga_2O_3 epitaxial films grown on the annealed substrates. Generally, μ increases with grain size due to reduced grain boundaries and thus suppressed grain-boundary scattering, especially for nanocrystalline materials. Moreover, μ is also sensitive to lattice imperfections, for example, vacancies, dislocations, and distortions [22, 23]. Therefore, μ values are larger due to better crystallinity and larger grains in the β-Ga_2O_3 epitaxial films grown on annealed substrates; these results are well-supported by the AFM and XRD results.

Optical Materials EXPRESS

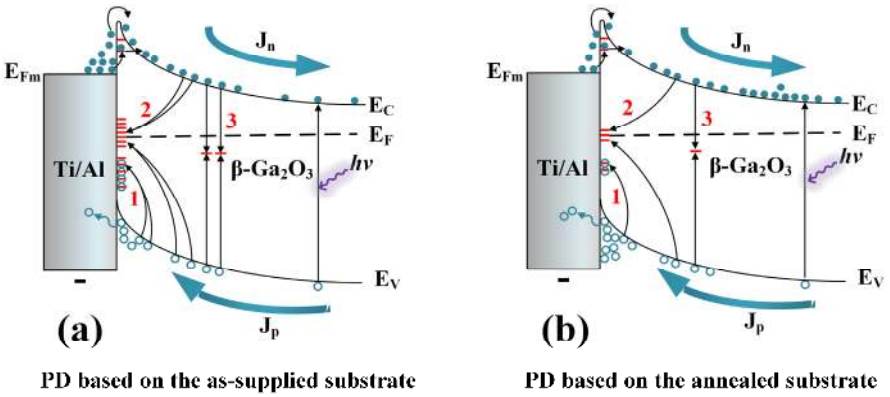

Fig. 5. Schematic energy band diagrams of the β-Ga_2O_3 MSM PD under DUV illumination based on (a) as-supplied substrate and (b) annealed substrate. E_C, E_F and E_V represent conduction-band energy, Fermi level and valence-band energy, respectively. The electron and hole current densities are referred to as J_n and J_p.

After exposure to DUV illumination, all PDs exhibited a considerable photoresponse with a significant current increase. Moreover, as shown in Fig. 4(b), the scales of the photocurrent (I_{photo}) are very close for all PDs except PD-1050, which demonstrates significant enhancement. For example, the I_{photo} values of PD-0, PD-600, PD-750, PD-900, and PD-1050 under the bias of 10 V are 0.517, 0.522, 0.500, 0.600, and 8.056 mA/cm^2, respectively. Accordingly, the responsivities (R) are 3.5 A/W, 3.6 A/W, 3.4 A/W, 4.1 A/W, and 54.9 A/W, respectively. I_{photo} and R are not improved as significantly as I_{dark}, even with enhanced μ and correspondingly more effective carrier transport in the β-Ga_2O_3 epitaxial film, unless the substrate-annealing temperature is raised to 1050 °C. In general, there is an internal gain (G) mechanism in MSM PDs due to the trapping of minority carriers at/near the metal/β-Ga_2O_3 interface (see process 1, Fig. 5), which often dominates the scale of responsivity [24]. G can be estimated by

$$G = Rhc/\eta q\lambda \tag{2}$$

where h is Planck's constant, c is the velocity of light, η is the quantum efficiency, q is the electron charge, and λ is the wavelength of the incident light [25]. Herein, the incident photons are assumed to be absorbed completely, that is, η = 100%. Then, the G values of PD-0, PD-600, PD-750, PD-900, and PD-1050 are 17.2, 17.4, 16.6, 20.0, and 268.2, respectively. In this work, the improved crystallinity of the β-Ga_2O_3 epitaxial films grown on annealed substrates reduces the structural-disorder-related defects, which can act as acceptor states [26, 27]. Next, the trapping of photogenerated holes is suppressed to some extent, as exhibited in Fig. 5(b), which slows the increase of G, even with enhanced μ. The sharp increase in photoresponse observed for PD-1050 with extremely high-temperature substrate-annealing is attributed to the combined effects of the dramatic increase in μ and the effective reduction in deep-level defects, which can act as recombination centers for non-equilibrium carriers (see processes 2 and 3, Fig. 5) [28]. Furthermore, as shown in Fig. 4(c), the un-synchronized increases in I_{dark} and I_{photo} result in a slight degradation of I_{photo}/I_{dark} for PDs based on annealed substrates. D* is another key figure-of-merit for PD, which describes the sensitivity, including both the photoresponse and the noise floor. D* is expressed as

$$D^* = R\sqrt{\frac{S}{2qI_{dark}}} \tag{3}$$

Optical Materials EXPRESS

where S is the effective area under illumination, with the shot noise from I_{dark} being regarded as the major contribution to the noise floor [29]. As shown in Fig. 4(d), the loss in D* is caused by adopting the annealed substrates, except for PD-1050, whose D* is increased by one order of magnitude compared to that of PD_0. These findings reveal that the substrate-annealing temperature has to be high enough to offset the impact of the I_{dark} increase. Table 1 lists several critical device metrics of the presently described and other previously reported thin-film-type β-Ga_2O_3 PDs. Clearly, the performance of PD-1050 is comparable to the best values reported in the literature. In particular, extremely high responsivity and detectivity were observed, which are even higher than those of the highly sensitive solar-blind PD based on a graphene/β-Ga_2O_3-wafer heterojunction (39.3 A/W and 5.92×10^{13} at 20 V) [30].

Table 1. Comparison on device performance of present device and other previously reported β-Ga_2O_3 MSM PDs. Bias voltage was 10 V, unless otherwise indicated.

Sample	I_{dark} (pA)	I_{photo} (μA)	I_{photo}/I_{dark}	R (A/W)	D* (Jones)	T_d (s)
PD-0 (this work)	4.4	0.093	2.11×10^4	3.5	5.78×10^{13}	0.56
PD-600 (this work)	8.5	0.094	1.11×10^4	3.6	4.20×10^{13}	0.88
PD-750 (this work)	8.8	0.090	1.02×10^4	3.4	3.95×10^{13}	1.08
PD-900 (this work)	9.8	0.108	1.10×10^4	4.1	4.50×10^{13}	0.80
PD-1050 (this work)	26.0	1.450	5.58×10^4	54.9	3.71×10^{14}	4.00
Ref. [13]	…	0.218@5 V	…	1.45@5 V	…	1.2/32.86
Ref. [15]	…	1.46	>10	…	…	1.02/16.61
Ref. [31]	12@5 V	1.8@5 V	1.5×10^5	0.903@5 V	…	<3
Ref. [32]	620@20 V	2.9@20 V	4.68×10^3	17@20 V	7.3×10^{12}	…

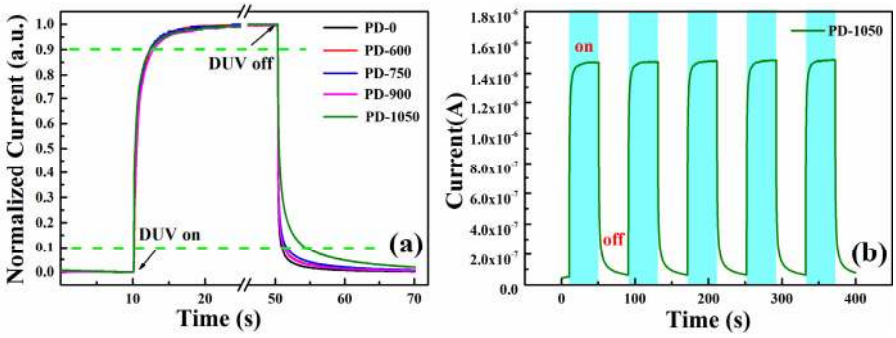

Fig. 6. Transient response of β-Ga_2O_3 PDs: (a) normalized responses of all the PDs and (b) multi-cycle response of PD-1050. During the measurement, 254-nm and 69.5-μW/cm^2 DUV light source was repeatedly switched on and off at 40-s time intervals, and bias was maintained at 10 V.

Figure 6(a) presents the normalized transient responses of the β-Ga_2O_3 PDs, from which both the rise time (T_r, defined as the time during which the current increases from 10% to 90% of the peak value) and the decay time (T_d, defined as the time during which the current decays from 90% to 10% of the peak value) are extracted for each PD [1, 2]. The recovery of the β-Ga_2O_3 PDs on the annealed substrates is much slower than that of PD-0 (T_d = 0.56 s), while there is no obvious difference in T_r (~2 s) among all PDs. In particular, PD-1050 exhibits the longest recovery time (T_d = 4.0 s), more than seven times longer than that for PD-0. As discussed above, the improved crystallinity of the β-Ga_2O_3 epitaxial films grown on

annealed substrates can reduce the structural-defect-induced traps and thus the persistent photoconductivity (PPC) because the slow process of carrier detrapping is suppressed [15]. Therefore, the prolonged recovery observed in this work is attributed to reduced recombination centers in the β-Ga_2O_3 epitaxial films grown on annealed substrates and thus longer non-equilibrium carrier lifetimes [33]. This effect is more significant for PD-1050, with the highest substrate-annealing temperature. These observations support the discussion on I-V characteristics. However, PD-1050 still exhibits good reproducibility and stability in operation, as shown in Fig. 6(b). In addition, it is possibly the trade-off between μ and carrier lifetime that results in the slight difference in T_r for all the samples. Figure 7 demonstrates the spectral responses of the PDs measured under 10-V bias, and their peak responses all occur at approximately 254 nm. PD-1050 possesses much higher responsivity than other samples throughout the whole solar-blind region, owing to the highest crystallinity in its β-Ga_2O_3 film. Furthermore, the rejection ratio (R_{254}/R_{350}), defined as the ratio of the responsivity values at 254 and 350 nm, of PD-1050 is 3.22×10^3, which is sufficiently large to guarantee true solar-blind photodetection.

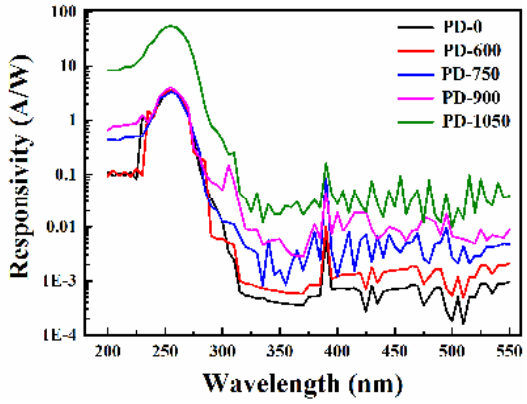

Fig. 7. Spectral responses of β-Ga_2O_3 MSM PDs based on sapphire substrates with different thermal-annealing pretreatments.

4. Conclusions

Thermal-annealing pretreatment on c-plane sapphire substrates was conducted in a tubular furnace, and the effects on both the structural properties of the β-Ga_2O_3 epitaxial film and the characteristics of related MSM PD were comprehensively investigated. Smoother surfaces and even a similar terrace-and-step morphology on substrates were achieved by the pretreatment, owing to the reconstruction of the surficial crystal structure. As a result, the crystallinity of the β-Ga_2O_3 epitaxial film was effectively improved, as indicated by the XRD and AFM results, which was more evident at higher annealing temperatures. Moreover, increases in both I_{dark} and I_{photo} were observed when using the annealed substrate, which were attributed to enhanced μ of more-crystallized films and fewer grain boundaries in the film. However, the substrate-annealing temperature must be sufficiently high that improvements in photodetection properties outweight the negative impact of the I_{dark} increase. As a result, PD-1050 presented extremely high sensitivity: high responsivity of 54.9 A/W and large D* of 3.71×10^{14} Jones. Both parameters were increased by one order of magnitude compared with those of PD-0. Such a sharp improvement was attributed to the combined effects of the dramatic μ increase and effectively reduced defect-related recombination centers. Nevertheless, the reduction of recombination centers resulted in a slower recovery for the PDs with annealed substrates, particularly for PD-1050. These findings demonstrate a new avenue for the development of highly sensitive β-Ga_2O_3 solar-blind PDs.

Optical Materials EXPRESS

Funding

National Natural Science Foundation of China (61504022).